

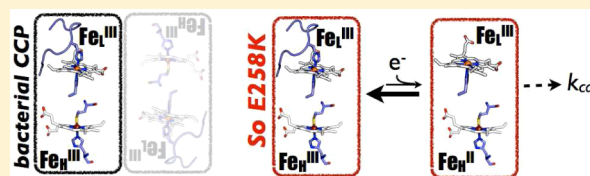
# Impact of Quaternary Structure upon Bacterial Cytochrome *c* Peroxidases: Does Homodimerization Matter?

Katie E. Ellis, Katherine E. Frato, and Sean J. Elliott\*

Department of Chemistry, Boston University, 590 Commonwealth Avenue, Boston, Massachusetts 02215, United States

## Supporting Information

**ABSTRACT:** All known active forms of diheme bacterial cytochrome *c* peroxidase (bCcP) enzymes are described by a homodimeric state. Further, the majority of bCcPs reported display activity only when the high-potential electron transfer heme of the protein ( $\text{Fe}_\text{H}$ ) is reduced to the ferrous oxidation state. Reduction of  $\text{Fe}_\text{H}$  results in a set of conformational changes allowing for the low-potential peroxidatic heme ( $\text{Fe}_\text{L}$ ) to adopt a high-spin, five-coordinate state that is capable of binding substrate. Here we examine the impact of dimerization upon the activity of the *Shewanella oneidensis* (So) bCcP by the preparation of single charge-reversal mutants at the dimer interface and use the resulting constructs to illustrate why dimerization is likely a requirement for activity in bCcPs. The E258K mutant is found to form a monomeric state in solution as characterized by size exclusion chromatography and analytical ultracentrifugation analyses. The resulting E258K monomer has an unfolding stability comparable to that of wild-type So bCcP and an activity that is only slightly diminished ( $k_\text{cat}/K_\text{m} = 23 \times 10^6 \text{ M}^{-1} \text{ s}^{-1}$ ). Spectroscopic and potentiometric analyses reveal that while the thermodynamic stability of the activated form of the enzyme is unchanged (characterized by the  $E_\text{m}$  value of the  $\text{Fe}_\text{H}^\text{II}/\text{Fe}_\text{H}^\text{III}$  couple), the kinetic stability of the activated form of the enzyme has been greatly diminished upon generation of the monomer. Together, these data suggest a model in which dimerization of bCcP enzymes is required to stabilize the lifetime of the activated form of the enzyme against reoxidation of  $\text{Fe}_\text{H}$  and deactivation of  $\text{Fe}_\text{L}$ .



Bacterial diheme cytochrome *c* peroxidase (bCcP) enzymes, which detoxify hydrogen peroxide in the periplasmic space of many Gram-negative bacteria by utilizing reducing equivalents from the cytochrome *c* redox pool,<sup>1–3</sup> have always been described as homodimeric enzymes. Each bCcP protomer contains two *c*-type heme cofactors and an additional  $\text{Ca}^{2+}$  ion, and eight different bCcP enzymes have been studied structurally through X-ray crystallographic analyses.<sup>4–12</sup> In all cases, bCcPs crystallize as homodimers, and the dimeric state has been further substantiated by hydrodynamic studies of several different bCcP enzymes.<sup>8,13–15</sup> In the case of the *Paracoccus denitrificans* (Pd) enzyme, conditions that stabilize homodimerization have been studied in some detail: it has been illustrated by Pettigrew and co-workers that removal of the  $\text{Ca}^{2+}$  or artificially low ionic strengths result in an inactive, monomeric form of the enzyme.<sup>14</sup>  $\text{Ca}^{2+}$  binding in bCcPs is thought to have two roles: a tight-binding  $\text{Ca}^{2+}$  affinity found in all bCcP enzymes that impacts electronic communication between the heme groups<sup>5,8,16,17</sup> and a nonspecific ionic strength effect that shifts the equilibrium between inactive monomers and active dimers toward the dimerized state, as described for the Pd and *Pseudomonas nautica* (Pn) enzymes.<sup>5,8,14</sup> However, the basis for why the dimeric state is required to achieve catalysis is poorly understood, and here we examine this issue in further detail using the enzyme from *Shewanella oneidensis* (So)<sup>11,18</sup> as a model system to generate a monomerized version of the protein that retains catalytic activity. Our results suggest an unforeseen role in dimerization

as a requirement to stabilize a conformation of the active site that is required for catalysis.

In contrast to the apparent required quaternary structure, the requirement for the cofactors in bCcPs is well-understood: the high-potential (200–450 mV vs NHE) Met-His ligated heme (H-heme) serves as a mediator of the transfer of electrons to the other, low-potential heme (approximately –300 mV vs NHE) that acts as the peroxidatic active site.<sup>3,19</sup> The  $\text{Ca}^{2+}$  ion is located at the interface between the H-heme and L-heme domains. The high-potential heme, which is not present in monoheme peroxidases (e.g., yeast CcP), is likely responsible for storing a second oxidizing equivalent during the catalytic cycle for many bCcP enzymes<sup>19</sup> and serving as an electron transfer conduit or mediator.<sup>20,21</sup> Despite these broadly conserved similarities, within bCcPs a functional difference in whether the isolated,  $\text{Fe}_\text{L}^\text{III}\text{Fe}_\text{H}^\text{III}$  oxidation state of the protein displays activity arises. Most characterized bCcPs are isolated in a catalytically inactive, fully oxidized ( $\text{Fe}_\text{L}^\text{III}\text{Fe}_\text{H}^\text{III}$ ) state, where the L-heme is *bis*-His coordinated such that substrate cannot bind to  $\text{Fe}_\text{L}$ .<sup>2–4</sup> The active form of the enzyme can be achieved by the addition of one electron to the H-heme. This reductive activation not only yields an  $\text{Fe}_\text{H}^\text{II}\text{Fe}_\text{L}^\text{III}$  oxidation state but also results in local conformational changes that cause the reorientation of ligands around the active site heme, producing

Received: August 24, 2012

Revised: November 22, 2012

Published: November 28, 2012



an “open” conformer that allows peroxide to bind at  $\text{Fe}_L$ . Collectively, these requirements have been illustrated for the canonical bCcP enzymes from *Pseudomonas aeruginosa* (Pa),<sup>4,33</sup> *P. denitrificans* (Pd),<sup>5</sup> *Ps. nautica* (Pn),<sup>6</sup> *Rhodobacter capsulatus* (Rc),<sup>7</sup> *Pseudomonas stutzeri* (Ps),<sup>8</sup> two isoenzymes from *Geobacter sulfurreducens* (Gs),<sup>9,10</sup> and, recently, *S. oneidensis* (So),<sup>11</sup> all of which require activation through the production of the  $\text{Fe}_H^{\text{II}}\text{Fe}_L^{\text{III}}$  oxidation state, to generate the open conformer. In contrast to this canonical family of diheme peroxidases, the enzymes from *Nitrosomonas europaea* (Ne)<sup>22</sup> and *Methylococcus capsulatus* Bath (Mc)<sup>15</sup> do not need to undergo an activation step: the as-isolated enzyme, still in the  $\text{Fe}_H^{\text{II}}\text{Fe}_L^{\text{III}}$  oxidation state, displays a pentacoordinate active site iron that is active without further reduction.<sup>12</sup> Regardless of the functional manifold displayed by bCcP enzymes, every known bCcP is a homodimer, suggesting that the dimeric state has an important, yet poorly understood, functional role. Here, we generate a charge-reversal mutant of the *Shewanella* enzyme to disrupt the protein dimer interface and address the question of why all bCcP enzymes are dimers.

## MATERIALS AND METHODS

**Protein Expression and Purification.** Recombinant *S. oneidensis* cytochrome *c* peroxidase was expressed and purified in the same manner as in the recent work by Pulcu et al.<sup>18</sup> Similarly, the recombinant *So*  $c_5$  (gene SO0264/plasmid pSOc5) was expressed and purified as described previously by Pulcu et al.<sup>18</sup> *So* CcP mutants, E258K and E321K, were constructed using the QuikChange Mutagenesis Kit and expressed and purified as MBP fusions as described for the wild-type enzyme. The glutamic acid residue at position 258 was mutated to lysine using the following primers: 5'-CCGACACTGCGCAATATTAACCTATCCCTAC-3' (forward) and 5'-GTAGGGATAGGTTAGTTTAATATTGCGCAGTGTCCG-3' (reverse). The presence of the correct mutations at position 258 was verified by gene sequencing (GeneWiz). This mutant required induction with 500  $\mu\text{g/L}$  IPTG for 4 h for optimal expression. Purification followed the same steps as that of wild-type CcP. The glutamic acid residue at position 321 was mutated to lysine using the following primers: 5'-CCACCATCAAATAAAAAGACTCCGCGCCCA-GTT-3' (forward) and 5'-AACTGGGCGCGGAGTCTTTT-TATTTGATGGTGG-3' (reverse). The presence of the correct mutations at position 321 was verified by gene sequencing. Expression and purification followed the same steps that were used for wild-type CcP.

**Chemical Monomerization.** Wild-type CcP was diluted to 50  $\mu\text{M}$  and dialyzed in 20 mM HEPES, 150 mM NaCl, and 10 mM EGTA (pH 8) for 4 h at room temperature. Buffer was then replaced and the dialysis continued overnight at 4 °C. Samples were concentrated to 25  $\mu\text{M}$  and applied to an S-100 column equilibrated with 20 mM HEPES, 150 mM NaCl, and 1 mM EGTA (pH 8). Fractions containing CcP were concentrated to approximately 100  $\mu\text{M}$ , and excess EGTA was removed by dialysis.

**Analytical Ultracentrifugation.** Sedimentation velocity AUC experiments were conducted using a Beckman XL-I analytical ultracentrifuge (Beckman Coulter) with an absorbance optical system at the Massachusetts Institute of Technology Biophysical Instrumentation Facility. Fresh samples of 10  $\mu\text{M}$  *So* CcP were extensively dialyzed against 20 mM HEPES and 50 mM NaCl (pH 7.5). The protein solution and dialysate were loaded into two-sector cells and

equilibrated thermally until a constant temperature of 20.0 °C was reached prior to centrifugation for  $\geq 10$  h at 42000 rpm. The protein concentration across the cell was measured by monitoring the heme absorbance at 420 nm at 2 min intervals. Data were analyzed using Sedfit, and diffusion-deconvoluted sedimentation coefficient distributions,  $c(s)$ , were generated from 200 scans with SedFit.34. The sedimentation coefficients were converted to standard values ( $s_{20,w}$ ) using a solvent viscosity of 1.0221 and a density of 1.00185 g/mL (calculated with Sednterp35).

**Thermal Denaturation Monitored by CD.** CD spectra of *S. oneidensis* wild-type CcP and charge-reversal mutant samples were recorded with an Applied Photophysics circular dichroism spectrophotometer with a Quantum Northwest temperature controller. Data were collected using a 0.1 mM path length anaerobic quartz cuvette. CcP enzyme samples were kept in 25 mM phosphate buffer (pH 7.0) at a final protein concentration of 20  $\mu\text{M}$ . At each given temperature (increased stepwise by 1 °C from 20 to 90 °C), the protein sample was allowed to equilibrate for 2 min before the intensity at 222 nm was recorded with an averaging time of 5 s/°C.

**Activity Assays.** The electronic absorption spectra of the CcP enzyme were collected on a Cary 50 spectrophotometer (Varian). All enzymatic assays were performed at 23 °C in standard assay buffer that consisted of 5 mM MES, 5 mM HEPES, 10 mM NaCl, and 1 mM  $\text{CaCl}_2$  (pH 6). Horse heart cytochrome *c* (Sigma) and *So* cytochrome  $c_5$  were reduced by being treated with 20 mM L-sodium ascorbate (Sigma), and excess reductant was removed using a PD-10 desalting column (NEB) before the assay. CcP stock solutions were reductively activated with 1 mM L-sodium ascorbate and 10  $\mu\text{M}$  diaminodulol (DAD) and incubated on ice in assay buffer for at least 30 min, which prepared the active,  $\text{Fe}_H^{\text{II}}\text{Fe}_L^{\text{III}}$ , form of the enzyme. The extent of reduction of the sample was monitored by optical absorption. The oxidations of the reduced horse heart cytochrome *c* and *So*  $c_5$  are monitored at 550 and 553 nm, respectively, in the presence of  $\text{H}_2\text{O}_2$  using an extinction coefficient difference between the oxidized and reduced proteins ( $\Delta\epsilon_{550} = 21.5 \text{ mM}^{-1} \text{ cm}^{-1}$  for horse heart cytochrome *c*, and  $\Delta\epsilon_{553} = 12.5 \text{ mM}^{-1} \text{ cm}^{-1}$  for cytochrome  $c_5$ ).<sup>18</sup>

**Potentiometric Redox Titrations.** Anaerobic redox titrations of the H-heme of *S. oneidensis* wild-type CcP and the E258K charge-reversal mutant were conducted and followed optically in the wavelength range of 300–800 nm. Titrations were performed at 23 °C by measuring absorption changes at 553 nm of 6  $\mu\text{M}$  protein solutions in 10 mM MES/HEPES (pH 6.0) in the presence of 2 mM  $\text{CaCl}_2$ . Redox potentials were measured using a combination Ag/AgCl Micro Redox electrode (MI-411, Microelectrodes, Inc.). The solution potential was adjusted using stepwise microliter additions of reductant (25 mM sodium dithionite) or oxidant (25 mM potassium ferricyanide). Diaminodulol and phenazine methosulfate were included as mediators at final concentrations of 15  $\mu\text{M}$  (inclusion of additional mediators did not improve or change the experimental results, so triple replicates with just the two mediators were generated).

**Oxidation and Reduction Kinetic Analysis of Wild-Type *So* CcP and E258K.** The rate of semireduction of the oxidized forms of the wild-type *So* enzyme and E258K charge-reversal mutant with L-sodium ascorbate and 1  $\mu\text{M}$  DAD was monitored at 408 and 553 nm at 23 °C using a Cary 50 spectrophotometer (Varian). Various concentrations of L-

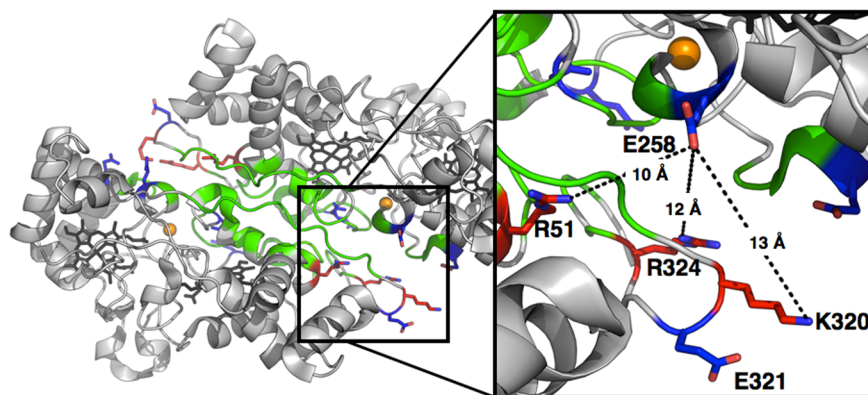


**Figure 1.** Crystal structure of *S. oneidensis* bCcP in the fully reduced oxidation state (PDB entry 3O5C). The dimer interface is highlighted by the colored residues predicted by PDBePISA and analysis of the crystal structure. Green residues represent uncharged interfacial amino acids; red residues are positively charged, and blue residues are negatively charged. The inset shows the local environment around residues E258 and E321. Potential long-range, charge pairing interactions with positively charged residues (R51, R320, and R324) are shown as dotted lines.

sodium ascorbate (1, 2.5, and 5 mM) were used to ensure pseudo-first-order kinetics applied to the reduction of 3  $\mu$ M wild-type *So* CcP and the E258K mutant.  $k_{\text{obs}}$  was then calculated according to pseudo-first-order kinetic parameters. Reoxidation of the activated enzyme was achieved by first desalting the semireduced enzymes anaerobically and then exposing the samples to an ambient atmosphere. The same wavelengths were monitored for the reoxidation as for the reduction.

## RESULTS

### Cytochrome *c* Peroxidase Dimer Interface Analysis.

The dimer interface of the *S. oneidensis* cytochrome *c* peroxidase crystal structure was analyzed using the Protein Data Bank Europe Protein Interfaces, Surfaces, and Assemblies tool (PDBePISA),<sup>23</sup> a web-based server for examining potential macromolecular interfaces and predicting probable quaternary structures as well as searching databases for structurally similar interfaces and assemblies. PDBePISA was used to predict the residues that form charged interactions across the dimer interface of the *So* enzyme (PDB entry 3O5C) and the other crystallized dimeric bCcP enzymes. The structure of the *So* enzyme<sup>24</sup> (in the fully reduced oxidation state) and the 11 other bCcP structures were analyzed and are listed in Table S1 of the Supporting Information. Eight different enzymes are crystallized as dimers, and between two and eight charged pairs are found across the dimer interfaces of the various enzymes. *So* CcP has six charged pairs in the semireduced enzyme. The interfacial location of E258 was confirmed by the crystal structure, shown in Figure 1, which illustrates that the charge-reversal mutation is in a position that would likely disrupt three long-range charge interactions (<10 Å) across the dimer interface. In comparison, E321 is only located in the proximity of the interface but lacks discernible charge interactions with the neighboring monomer (Figure 1), providing a negative control for comparisons between characteristics of E258K that might not be linked to the potential disruption of the dimer interface.

**Hydrodynamic Properties of the Dimer and Monomer Enzymes.** To verify that installation of the E258K mutation resulted in the generation of a monomeric version of *So* CcP, size exclusion chromatography was used to observe the changes in the quaternary structure of the various forms of *So* CcP (i.e., monomer vs dimer). The chromatograms in Figure 2 show the

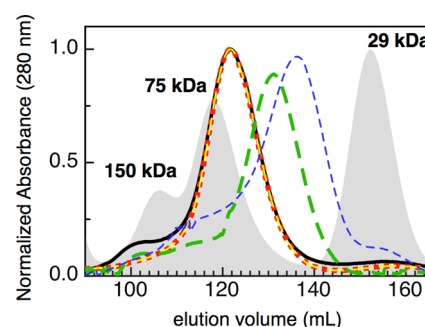


**Figure 2.** Molecular size exclusion chromatography of *S. oneidensis* CcP, with respect to standards (gray). As-isolated *So* CcP (solid black) eluted with an apparent molecular mass of 67 kDa. The enzyme incubated with 10 mM  $\text{CaCl}_2$  (red dots) eluted with an apparent molecular mass equal to that of the untreated form, whereas the enzyme treated with EGTA (dashed green) elutes with an apparent molecular mass of 43 kDa. The as-isolated E258K (dashed blue) elutes with a significantly lower apparent mass (32 kDa). The as-isolated E321K (dashed yellow) displays an apparent molecular mass of 67 kDa.

elution profiles for the various *So* enzymes under different treatment conditions: as-isolated wild-type enzyme (solid black), incubated with EGTA (green), and as-isolated E258K (blue). The as-isolated sample of the wild-type protein eluted with an apparent molecular mass ( $M_r$ ) of 67 kDa, consistent with the dimeric state of the enzyme. In the presence of excess calcium (1 mM  $\text{CaCl}_2$ , red dots), the elution profile of the wild-type protein does not change: it is the same as that of the as-isolated sample. In contrast, evidence of higher-order oligomers has been previously found for the *Ps* enzyme in the presence of excess  $\text{Ca}^{2+}$ ,<sup>8</sup> and in the presence of 1 mM EGTA, all bCcPs examined here display an  $M_r$  of 43 kDa (dashed green line in Figure 2), correlating to a monomeric form of the protein. The apparent discrepancy between the observed  $M_r$  and the theoretical size of the monomer can be explained by a difference in the shape of the chemically monomerized protein sample and a theoretical monomeric enzyme, as discussed in further detail below.

Size exclusion chromatography was used to observe the changes in quaternary structure of the E258K and E321K charge-reversal mutants to determine the conditions under which the charge-reversal mutants are monomers or dimers.



The chromatograms in Figure 2 show the elution profiles for the E258K (blue) and E321K (yellow) charge-reversal mutants under the same treatment conditions as the wild-type enzyme. The as-isolated E258K sample elutes with an  $M_r$  of 32 kDa. This is consistent with the monomeric state of the protein sample. In the presence of either excess calcium or EGTA, the  $M_r$  of E258K is equal to that of the as-isolated sample with an apparent  $M_r$  of 32 kDa, which correlates to a monomeric form of the protein (data not shown). The as-isolated E321K sample elutes with an  $M_r$  of 67 kDa. This is consistent with the dimeric state of the protein sample.

The sedimentation velocity profiles for as-isolated *So* bCcP in the presence of excess  $\text{Ca}^{2+}$  or EGTA were analyzed by the DCDT+ method.<sup>25</sup> The sedimentation coefficient distributions are shown in Figure 3, where the maximal  $s_{20,w}$  value of the as-

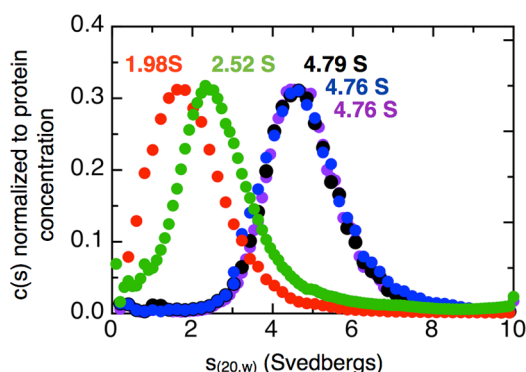


**Figure 3.** Sedimentation velocity analytical ultracentrifugation (AUC). AUC of *S. oneidensis* CcP shows the effect of a charge-reversal mutation at the dimer interface: as-isolated bCcP (black), EGTA-treated bCcP (green), E258K (red), E321K (blue), and bCcP with  $\text{Ca}^{2+}$  (purple). The distributions are calculated from the 420 nm absorbance. No minor species were observed, indicating that the charge-reversal mutation and EGTA treatment completely monomerized the enzyme samples.

isolated, wild-type *So* CcP is 4.79 S, nearly identical to values reported for other dimeric bCcP enzymes (Table 1).<sup>8,13–15</sup>

**Table 1. Sedimentation Coefficients of Dimeric and Monomeric bCcP Enzymes**

enzyme	sedimentation coefficient (S)		ref
	dimer	monomer	
<i>Ps. stutzeri</i>	4.67	2.83	8
<i>P. denitrificans</i>	4.78	2.69/2.54	14
<i>Paracoccus pantotrophus</i>	4.8	ND <sup>a</sup>	13
<i>M. capsulatus</i>	4.82	ND <sup>a</sup>	15
<i>S. oneidensis</i>	4.79	2.52/1.98	this work

<sup>a</sup>Not determined.

Preparation of the  $\text{Ca}^{2+}$ -depleted enzyme and sedimentation in the presence of EGTA yield an  $s_{20,w}$  value 2.52 S, consistent with those of other chemically monomerized, EGTA-treated enzymes.<sup>8,21</sup> Treating the apoprotein with excess  $\text{Ca}^{2+}$  leads to the return of the native hydrodynamic traits: the presence of excess  $\text{Ca}^{2+}$  results in a maximal  $s_{20,w}$  of 4.76, essentially identical to the value of the wild-type protein.

The sedimentation velocity profiles for the as-isolated E258K charge-reversal mutant (as-isolated enzyme, enzyme in the

presence of excess  $\text{Ca}^{2+}$ , or EGTA-treated enzyme) were analyzed using the same method used for wild-type *So* bCcP (Figure 3). The  $s_{20,w}$  value of as-isolated E258K is 1.98 S. The presence of either an excess of  $\text{Ca}^{2+}$  or EGTA does not change the  $s_{20,w}$  value (data not shown). All of the  $s_{20,w}$  values obtained for the E258K variant are consistent with a protein of molecular mass of the monomer and suggest a further compacted structure for the E258K mutant versus the EGTA-treated wild-type enzyme. The sedimentation velocity profiles for the as-isolated E321K charge-reversal mutant were analyzed using the same method that was used for wild-type *So* bCcP (Figure 3). The  $s_{20,w}$  value of as-isolated E321K is 4.76 S, virtually identical to that of the wild-type as-isolated enzyme sample. Notably, the data are in agreement with the calculated values of  $s_{20,w}$  as determined by SOMO,<sup>26</sup> where the PDB file for the *So* bCcP crystal structure can be used to calculate values of 4.81 and 3.08 S, respectively.

**Thermal Denaturation Monitored by CD.** To further verify that the changes in the observed quaternary structure did not represent global unfolding of the protein, CD measurements were conducted to assess the stability of the wild-type and mutant enzymes. Thermal denaturation of wild-type *So* bCcP and E258K and E321K mutants was monitored at 222 nm, and the loss of the far-UV CD signal was used to monitor the temperature dependence of thermal denaturation (Figure 4). In all cases, it was found that thermal unfolding was not

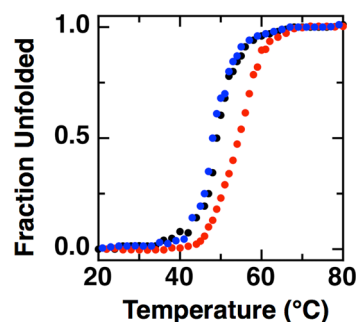


**Figure 4.** Thermal denaturation of *So* cytochrome *c* peroxidases monitored by CD. Typical curves of the fraction of unfolded enzyme measured at 222 nm as a function of temperature plotted for wild-type *So* CcP (black) and E258K (red) and E321K (blue) charge-reversal mutants. Samples consisted of 10  $\mu\text{M}$  peroxidase in phosphate buffer (pH 7.0).

freely reversible: the CD-detected protein melts led to partial, irreversible aggregation following unfolding, because of extended periods of time at elevated temperatures ( $>70^\circ\text{C}$ ). However, the unfolding experiments allow for the direct comparison of the stability of the wild-type and mutant proteins. At pH 7.0, a single unfolding transition was observed at a melting temperature ( $T_m$ ) of  $49.2 \pm 0.6^\circ\text{C}$  for the wild-type enzyme (Figure 4A), compared to the single unfolding transitions seen for the E258K and E321K charge-reversal mutants showing  $T_m$  values of  $53.9 \pm 0.3$  and  $48.3 \pm 0.4^\circ\text{C}$ , respectively. While it is surprising that disruption of the dimeric interface leads to a slight stabilization in the temperature of melting, the unforeseen enhancement of thermal stability upon monomerization suggests that the native protein may be less stable to account for its native processing and turnover in vivo, but clearly, the single-amino acid changes have not resulted in significant perturbations to the thermal stability of the tertiary structure of either the E258K or E321K mutant.

Table 2. Steady State Kinetic Characterization of E258K and E321K *So* bCcP Mutants

electron donor	parameter	wild type		E258K		E321K	
		semireduced	oxidized	semireduced	oxidized	semireduced	oxidized
horse heart cyt <i>c</i>	$K_m$ ( $\mu$ M)	$0.03 \pm 0.01$	$0.07 \pm 0.01$	$0.4 \pm 0.1$	no activity	$0.1 \pm 0.02$	$0.9 \pm 0.2$
	$k_{cat}$ ( $s^{-1}$ )	$1.9 \pm 0.2$	$1.3 \pm 0.1$	$0.7 \pm 0.1$		$5.1 \pm 0.2$	$3.5 \pm 1.0$
	$k_{cat}/K_m$ ( $\times 10^6$ $M^{-1} s^{-1}$ )	74	7.5	2		51	4
<i>So</i> cyt <i>c</i> <sub>5</sub>	$K_m$ ( $\mu$ M)	$0.3 \pm 0.1$	$0.6 \pm 0.5$	$0.8 \pm 0.1$	$0.7 \pm 0.2$	$0.4 \pm 0.1$	$0.8 \pm 0.3$
	$k_{cat}$ ( $s^{-1}$ )	$73 \pm 5$	$7 \pm 5$	$18 \pm 1$	$2.0 \pm 0.4$	$84 \pm 4$	$6 \pm 3$
	$k_{cat}/K_m$ ( $\times 10^6$ $M^{-1} s^{-1}$ )	240	12	23	3	210	8

### Catalytic Properties of the Charge-Reversal Monomer Mutant.

The activity of *So* CcP was determined previously in the presence of micromolar concentrations of various redox partner proteins,<sup>18</sup> where *So* cyt *c*<sub>5</sub> is the native electron donor in the periplasm of *Shewanella*<sup>27</sup> and horse heart cyt *c* can be used as an artificial electron donor that allows facile comparisons with other bCcP enzymes reported in the literature. Here, we determined kinetic parameters for the E258K and E321K charge-reversal mutants (Table 2). The linear initial rates at various peroxide concentrations were used to calculate kinetic parameters using the Michaelis–Menten formalism. As previously described for the wild-type enzyme, the electron donor proteins bind extremely weakly to *So* bCcP ( $K_m \gg 10 \mu$ M), and we could not achieve saturating concentrations *in vitro* using either electron donor that was studied: as a result, the values reported below are not maximal turnover rates.<sup>18</sup> As found previously with the wild-type enzyme, the kinetic parameters for both the E258K and E321K mutants depend on the electron donor used. The E321K mutant behaves overall like the wild-type enzyme displaying similar values of both  $k_{cat}$  and  $K_m$ . Overall, the E258K mutant shows a decreased  $k_{cat}$  under all conditions (3-fold lower), with respect to that of the wild-type protein, but still shows the enhanced kinetic parameters when *So* cyt *c*<sub>5</sub> is used as the electron donor, versus horse heart cyt *c*. With wild-type *So* bCcP, when horse heart cyt *c* is used as the electron donor, turnover is slowed by a factor of 30 compared to that of the native electron donor. For semireduced (activated) E258K, turnover with horse heart cyt *c* is approximately 20 times slower than reactions with the native electron donor cyt *c*<sub>5</sub>. Further, fully oxidized E258K displays no reactivity with horse heart cyt *c*.  $K_m$  values increase for E258K in all circumstances, increasing by 2–10-fold. Taken together, under the most efficient catalytic conditions for the wild-type enzyme (prereduced with ascorbate, using native *So* cyt *c*<sub>5</sub> as the electron donor), E258K shows an order of magnitude loss in  $k_{cat}/K_m$  ( $23 \times 10^6 M^{-1} s^{-1}$ ), indicating that regardless of spectroscopic changes detailed above, the monomeric enzyme is kinetically competent, albeit with a somewhat diminished catalytic efficiency.

We have previously observed that assay progress curves initiated with the fully oxidized enzyme revealed a lag phase, which has been interpreted in terms of a kinetic model in which *in situ* conversion of the oxidized (inactive) state of the enzyme to the active state can occur, allowing for the extraction of a rate constant associated with the activation process.<sup>18</sup> The fully oxidized forms of both charge-reversal mutants also show such lag phase kinetics, and fitting with our kinetic model confirms the results from Michaelis–Menten analysis. Using this model, we have previously shown that *So* bCcP has an activation rate of  $0.07 \pm 0.02 s^{-1}$  when cytochrome *c*<sub>5</sub> is used as the electron donor with the fully oxidized wild-type enzyme.<sup>18</sup> For the charge-reversal mutants, the apparent activation rates are

essentially the same for E258K ( $0.05 \pm 0.01 s^{-1}$ ) and within a factor of 2 for E321K ( $0.03 \pm 0.01 s^{-1}$ ). In contrast, there are greater differences in the apparent turnover numbers. For fully oxidized wild-type *So* bCcP, the peroxide turnover rate calculated with the lag phase model is  $7 \pm 1 s^{-1}$  for the dimeric E321K mutant [similar to that ( $2 \pm 1 s^{-1}$ ) of the wild type], while for the monomerized E258K mutant, the turnover number is diminished by 50-fold ( $0.33 \pm 0.02 s^{-1}$ ). Together, these data suggest that E258K is less active, though possibly because of weaker binding of cyt *c*<sub>5</sub> to the E258K monomer mutant protein, or in a conformation that gives less efficient electron transfer versus that seen with the wild-type enzyme.

### Spectroscopic Properties of the E258K Charge-Reversal Mutant in Terms of Optical Absorption.

To assess the possible basis for the changes in catalytic properties, we first examined the optical characteristics of the charge-reversal mutants. The optical absorbance spectra of fully oxidized and ascorbate-reduced *So* bCcP, E258K, and E321K are shown in Figure 5. For the oxidized ( $Fe_H^{III}Fe_L^{III}$ ) form of each of the enzymes, the spectral features are virtually identical, including those of the EGTA-treated enzyme (data not shown). All fully oxidized samples have the characteristic Soret maximum at 407 nm and broad  $\alpha$  and  $\beta$  bands at 553 and 540 nm, respectively, that are typical for the *So* CcP enzyme.<sup>18</sup> As reported previously, upon reduction with L-sodium ascorbate, the Soret band of the wild-type enzyme shifts to 417 nm and a shoulder appears at 407 nm, while the  $\alpha$  and  $\beta$  bands at 553 and 540 nm, respectively, become sharper, consistent with the reduction of the H-heme.<sup>5</sup> The appearance of a charge transfer band at 640 nm (Figure 5, insets) suggests a high-spin ferric heme state.<sup>28</sup> In contrast, similar treatment of E258K with ascorbate causes the Soret band to shift to 417 nm, but with a poorly resolved shoulder at 407 nm; the  $\alpha$  and  $\beta$  bands at 553 and 540 nm, respectively, appear as with the wild-type enzyme, but the 640 nm band is absent (Figure 5B). The shoulder at 640 nm indicative of high-spin Fe(III) is known to be a feature of weak intensity, such that quantitation of the HS state has not been achieved in bCcP enzymes.<sup>16,18,29–31</sup> Thus, one impact of monomerization displayed by E258K is the decrease in the concentration of the  $Fe_L^{III}$  HS state, which is presumably required for binding  $H_2O_2$ .

**Potentiometric Redox Titrations.** While the optical measurements indicated that the semireduced form of E258K did not possess a high-spin, five-coordinate heme that could bind  $H_2O_2$ , the kinetic data indicate that the enzyme engages in catalysis though impeded, and therefore, E258K must bind peroxide. To better rationalize the kinetic differences between the constructs, we examined the electron transfer properties of the H-heme in the charge-reversal mutants. Oxidative and reductive titrations of  $Fe_H$  were conducted for both the wild type and the E258K charge-reversal monomerization mutant using potentiometry (Figure S1 of the Supporting Informa-

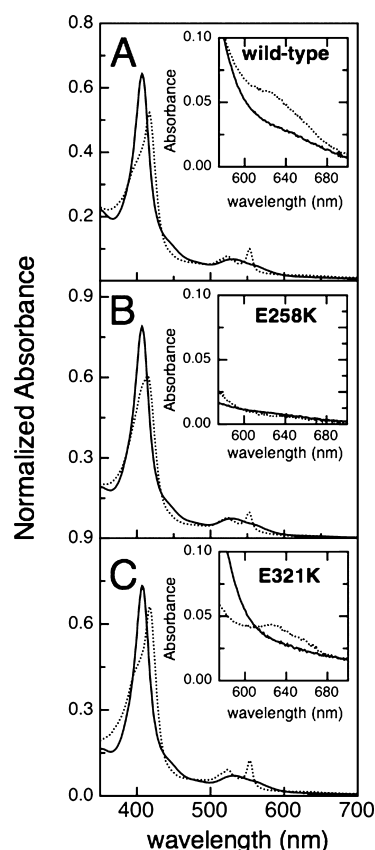


**Figure 5.** Electronic absorption spectra of oxidized (solid) and ascorbate-reduced (dot) (A) wild-type *So* bCcP, (B) the E258K charge-reversal mutant, and (C) the E321K mutant. The insets show the absorption spectra of oxidized and semireduced bCcP at a 5-fold higher concentration.

tion). Because of the large separation in potential between the high-potential heme and low-potential heme found in bacterial cytochrome *c* peroxidases, the contribution of the higher-potential heme can be easily isolated.<sup>15,17,19,29</sup> Reductive and oxidative titrations of the  $\text{Fe}_\text{H}^\text{II}/\text{Fe}_\text{H}^\text{III}$  couple for the wild-type *So* enzyme yielded an  $E_\text{m}$  value of  $246 \pm 1$  mV (vs SHE, at pH 6.0). E258K displayed lower potentials with slight hysteresis in the oxidative and reductive directions: reductive and oxidative titrations yielded redox potentials of 218 and 201 mV versus SHE, respectively. In all cases, Nernst plots showed slopes of  $\sim 59$  mV/decade, indicating that simple one-electron, one-proton processes are at work.

#### Kinetics of Ascorbate Reduction, and Air Reoxidation.

Though the E258K mutant possesses an H-heme with a slightly depressed reduction potential, the possible impact upon catalytic parameters was not evident, as a decrease of roughly 35 mV in the H-heme  $\text{Fe}^\text{II}/\text{Fe}^\text{III}$  redox potential should not impact its ability to reduce intermediates that might be generated in the course of peroxidatic chemistry or receive reducing equivalents from forms of cyt *c*. To address this issue, we examined the kinetic stability of the so-called “semireduced” state. In addition to the distinct Soret and 640 nm band features reported for E258K, the kinetics associated with ascorbate reduction of the fully oxidized enzyme to produce the  $\text{Fe}_\text{H}^\text{II}\text{Fe}_\text{L}^\text{III}$  state and the subsequent reoxidation with air were found to differ between the wild type and the charge-reversal mutant of *So* bCcP. Rates of ascorbate reduction and reoxidation of the enzymes were examined using the absorption

features described above (408 and 553 nm), as shown in Figure 6.

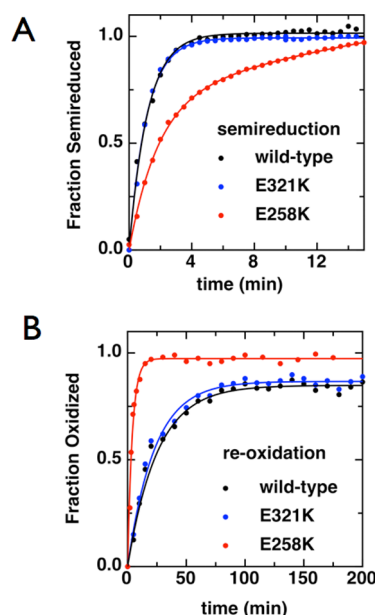


**Figure 6.** Kinetics of semireduction (top) and reoxidation (bottom) of wild-type bCcP (black) and the charge-reversal mutants, E321K (blue) and E258K (red), monitored at 553 nm. Assays were conducted using 3  $\mu\text{M}$  enzyme in 5 mM HEPES, 5 mM MES, 10 mM NaCl, and 1 mM  $\text{CaCl}_2$  (pH 6) at 23  $^\circ\text{C}$ . Data were fit to a pseudo-first-order model assuming the oxidant concentration is constant.

For the wild-type enzyme, reduction of 3  $\mu\text{M}$  bCcP with 5 mM L-sodium ascorbate (pseudo-first-order conditions) was monitored at either 553 or 408 nm, with reduction being achieved in minutes ( $k_\text{obs} = 0.90 \pm 0.03 \text{ min}^{-1}$  at 553 nm, and  $k_\text{obs} = 0.97 \pm 0.02 \text{ min}^{-1}$  at 408 nm). Similar time scales were required for reduction of E258K, though the final spectral features (i.e., Figure 4B) never exactly mimic those of the wild-type enzyme ( $k_\text{obs} = 0.36 \pm 0.02 \text{ min}^{-1}$  at 553 nm, and  $k_\text{obs} = 0.63 \pm 0.04 \text{ min}^{-1}$  at 408 nm). In contrast, reoxidation of the ascorbate-reduced enzyme proceeded on distinctly different time scales. As illustrated in Figure 6 (bottom), by first removing all exogenous reductant and then exposing the enzyme to atmospheric oxygen, we regenerated the fully oxidized spectrum on the order of hours (after the removal of excess ascorbate and DAD,  $k_\text{obs} = 0.04 \text{ min}^{-1}$ ), requiring up to days for full transformation of the 553 nm bands. E321K closely mimicked the wild-type enzyme. However, similar reoxidations of E258K were an order of magnitude faster than those with the wild type, occurring on the order of minutes ( $k_\text{obs} = 0.25 \text{ min}^{-1}$ ). Thus, upon monomerization, the  $\text{Fe}_\text{H}^\text{II}\text{Fe}_\text{L}^\text{III}$  state of the E258K mutant appears to be much less kinetically stable, unlike the stable, static “activated” conformation of bCcPs that has been amenable to crystallographic analyses.<sup>4,16,32</sup>

## DISCUSSION

The formation of homomultimeric structures is found throughout biology, where alternate quaternary structures can play key roles in assisting with overall folding stability,<sup>34–36</sup> producing allosteric affects for small molecule binding,<sup>36–38</sup> developing high localized concentrations, and allowing for alternate (“moonlighting”) activities.<sup>36,39,40</sup> In the case of bCcP



enzymes, homomultimerization is correlated to activity,<sup>8,29</sup> with all structurally characterized bCCPs being demonstrated to be (at least) homodimers. However, the apparent requirement for homodimerization has not been examined in detail previously. While canonical bCCP enzymes must undergo changes in secondary and tertiary structure that are tied to changes in the oxidation state of the H-heme and result in an open conformation at  $\text{Fe}_L$ , the apparent correlation between quaternary structure and activity has not been examined. To address this open question, we have produced the first, active monomeric version of a bCCP enzyme to allow us to ask the question of why all bCCPs are dimers. Through the analysis of the structurally conserved dimer interface among the eight different bCCP enzymes that have been crystallized to date, we have found that a single charge-reversal mutation, E258K, results in an active yet monomeric form of the traditionally dimeric enzyme. Notably, not all charge-reversal mutations generate a monomerized protein, as the E321K mutant still retains a homodimeric structure as determined by size exclusion chromatography and analytical ultracentrifugation.

In several respects, it is easier to report on what homodimerization does not impact. For example, wild-type *So* bCCP does not display allostery, half-site reactivity, or moonlighting activities, and the corresponding charge-reversal constructs reported here do not evince such properties. Many traits of E258K mimic those of the wild-type protein: the global folding stability of E258K is equal to or better than that of the wild-type protein; by some spectroscopic measures (e.g., fully oxidized optical spectrum), E258K is identical to the wild type; the reduction potential of the H-heme is modestly more negatively shifted (by 35 mV); and  $k_{\text{cat}}$  and  $K_m$  are affected, but not dramatically so. In terms of activity, the catalytic parameters listed in Table 2 reveal that the loss of activity displayed by E258K may be due to fundamental changes in catalytic events at the active site or may be due to changes in the ability of electron donors to interact with the enzyme. Thus, we conclude that E258K still acts as a reasonable cytochrome *c* peroxidase with the native electron donor, where  $k_{\text{cat}}/K_m$  values are similar to those found in other bacterial peroxidases.<sup>18</sup>

Given these observations, what might homodimerization achieve? The critical differences emerge in the optical spectrum of the semireduced enzyme ( $\text{Fe}_H^{\text{II}}\text{Fe}_L^{\text{III}}$ ), where  $\text{Fe}_L$  has undergone a change in conformation from being six-coordinate with His71 bound to an open conformation that displays activity. In the native enzyme, the semireduced form displays absorption features at ~550 nm indicative of the reduction of  $\text{Fe}_H$ , but also a weak feature at 650 nm that has been interpreted in terms of a high-spin ferric  $\text{Fe}_L^{\text{III}}$ . When the same state is prepared with E258K, the former features are present but the latter is absent, indicating that while  $\text{Fe}_H$  is reduced readily by ascorbate,  $\text{Fe}_L$  has most likely not undergone the requisite conformational change to an appreciable extent. The other key difference is found in the relative kinetics associated with the preparation and subsequent reoxidation (by air) of the  $\text{Fe}_H^{\text{II}}\text{Fe}_L^{\text{III}}$  state: while the wild type and E258K are similar in terms of the time scales associated with the reduction of the totally oxidized enzyme (by monitoring either the Soret region or the  $\alpha$  and  $\beta$  bands), they are hugely different when considering the reoxidation. The wild-type  $\text{Fe}_H^{\text{II}}\text{Fe}_L^{\text{III}}$  state is stable when it is exposed to air for hours to days, yet the monomerized E258K protein is reoxidized in seconds (i.e., less than a minute). This phenomenon does not seem to be entirely controlled by the actual reduction potential of the H-heme:

E258K has a potential only 35 mV lower than that of the wild type, and clearly, both H-heme centers should be readily oxidized by oxygen. The possible kinetic instability of the  $\text{Fe}_H^{\text{II}}\text{Fe}_L^{\text{III}}$  state in a monomerized bCCP is further corroborated by steady state kinetic analysis of the fully oxidized protein, where the decrease in the peroxide turnover rate can be interpreted in terms of a real-time decrease in the concentration of the activated form of the protein, because of its inactivation on the time scale of seconds (i.e., kinetic instability of the  $\text{Fe}_H^{\text{II}}\text{Fe}_L^{\text{III}}$  state in E258K leads to deactivation that competes with catalytic processes).

A full structural perspective of the relationship between the quaternary structure and the kinetic behavior described here requires a structure of E258K, yet without those data, inspection of the structures of activated dimeric forms of bCCP enzymes suggests that quaternary structure may play a role in achieving kinetic stabilization of the  $\text{Fe}_H^{\text{II}}\text{Fe}_L^{\text{III}}$  state as proposed here. One of the elements of the dimer interface is comprised by a single loop that contains the His71 residue responsible for ligating the peroxidatic heme iron in the “closed” form of the active site.<sup>4,11,12,16</sup> This loop structure (termed loop 1 by Einsle and co-workers<sup>9</sup>) packs against the second protomer in the dimeric structure, as shown in Figure 7.

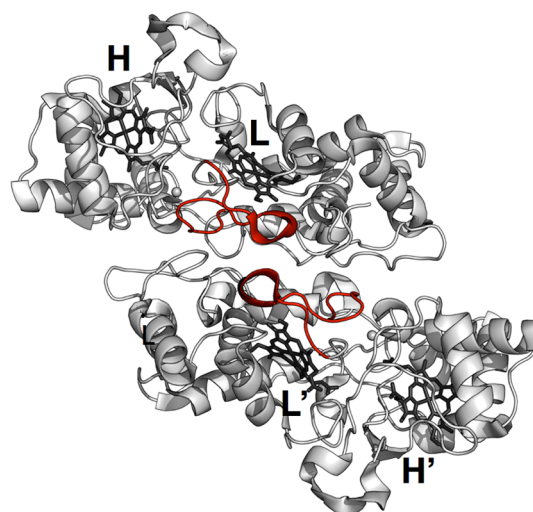


**Figure 7.** Depiction of loop 1 (red) of each bCCP protomer in the *So* wild-type enzyme (PDB entry 3OSC<sup>11</sup>). Loop 1 contains His71 that acts as a ligand at  $\text{Fe}_L$  in the closed form. However, in all structures of active enzymes, loop 1 adopts an open conformer that packs against the adjacent loop 1 of the second protomer in the dimer.

Without the presence of the second protomer molecule, loop 1 may engage in conformational dynamics, generating either open or closed forms of the active site and contributing to the overall kinetic instability of the activated  $\text{Fe}_H^{\text{II}}\text{Fe}_L^{\text{III}}$  state.

## CONCLUSIONS

Here we have demonstrated that without removal of the obligate  $\text{Ca}^{2+}$  ion found in the bCCP family, a charge-reversal monomeric construct can be prepared through destabilization of the interface between homodimers. Collectively, our data indicate that homodimerization of bCCPs is not significant for maintaining global folding energies but is for stabilizing the kinetic lifetime of the open,  $\text{Fe}_H^{\text{II}}\text{Fe}_L^{\text{III}}$  state that is the entry point for  $\text{H}_2\text{O}_2$  binding and peroxidase chemistry. Thus, it appears that the bCCP family (including the constitutively

active *Ne* enzyme) has maintained homodimeric quaternary structures to stabilize not the global protein fold, but the specific open conformation at Fe<sub>L</sub> that is needed for catalysis. One may infer that if bCcp protomers exist *in vivo*, they may be more prone to “deactivate” on a time scale of minutes.

## ■ ASSOCIATED CONTENT

### ■ Supporting Information

PDBePisa analysis and potentiometric titrations. This material is available free of charge via the Internet at <http://pubs.acs.org>.

## ■ AUTHOR INFORMATION

### Corresponding Author

\*Department of Chemistry, Boston University, 590 Commonwealth Ave., Boston, MA 02215. E-mail: [elliott@bu.edu](mailto:elliott@bu.edu). Telephone: (617) 358-2816. Fax: (617) 353-6466.

### Funding

This work was supported by National Institutes of Health Grant R01-GM072663 to S.J.E. and National Science Foundation Grant CHE 0840418.

### Notes

The authors declare no competing financial interest.

## ■ ABBREVIATIONS

bCcp, bacterial cytochrome *c* peroxidase; Fe<sub>H</sub>, high-potential heme; Fe<sub>L</sub>, low-potential heme; Pd, *P. denitrificans*; NHE, normal hydrogen electrode; Pa, *Ps. aeruginosa*; Pn, *Ps. nautica*; Rc, *R. capsulatus*; Ps, *Ps. stutzeri*; Gs, *G. sulfurreducens*; So, *S. oneidensis*; Ne, *N. europaea*; Mc, *M. capsulatus* (Bath); IPTG, isopropyl β-D-1-thiogalactopyranoside; HEPES, 4-(2-hydroxyethyl)-1-piperazineethanesulfonic acid; EGTA, ethylene glycol tetraacetic acid; AUC, analytical ultracentrifugation; CD, circular dichroism; MES, 2-(*N*-morpholino)ethanesulfonic acid; DAD, diaminodulol; PMS, phenazinemetosulfate.

## ■ REFERENCES

- (1) Van Spanning, R. J.; De Boer, A. P.; Reijnders, W. N.; Westerhoff, H. V.; Stouthamer, A. H.; and Van Der Oost, J. (1997) FnrP and NNR of *Paracoccus denitrificans* are both members of the FNR family of transcriptional activators but have distinct roles in respiratory adaptation in response to oxygen limitation. *Mol. Microbiol.* 23, 893–907.
- (2) Attack, J. M., and Kelly, D. J. (2007) Structure, mechanism and physiological roles of bacterial cytochrome *c* peroxidases. *Adv. Microb. Physiol.* 52, 73–106.
- (3) Pettigrew, G. W., Echalié, A., and Pauleta, S. R. (2006) Structure and mechanism in the bacterial dihaem cytochrome *c* peroxidases. *J. Inorg. Biochem.* 100, 551–567.
- (4) Echalié, A., Goodhew, C. F., Pettigrew, G. W., and Fulop, V. (2006) Activation and catalysis of the di-heme cytochrome *c* peroxidase from *Paracoccus pantotrophus*. *Structure* 14, 107–117.
- (5) Gilmour, R., Goodhew, C. F., Pettigrew, G. W., Prazeres, S., Moura, J. J., and Moura, I. (1994) The kinetics of the oxidation of cytochrome *c* by *Paracoccus* cytochrome *c* peroxidase. *Biochem. J.* 300, 907–914.
- (6) Alves, T., Besson, S., Duarte, L. C., Pettigrew, G. W., Girio, F. M., Devreese, B., Vandenberghe, L., Van Beeumen, J., Fauque, G., and Moura, I. (1999) A cytochrome *c* peroxidase from *Pseudomonas nautica* 617 active at high ionic strength: Expression, purification and characterization. *Biochim. Biophys. Acta* 1434, 248–259.
- (7) De Smet, L., Savvides, S. N., Van Horen, E., Pettigrew, G., and Van Beeumen, J. J. (2006) Structural and mutagenesis studies on the cytochrome *c* peroxidase from *Rhodobacter capsulatus* provide new insights into structure-function relationships of bacterial di-heme peroxidases. *J. Biol. Chem.* 281, 4371–4379.

- (8) Timoteo, C. G., Tavares, P., Goodhew, C. F., Duarte, L. C., Jumel, K., Girio, F. M., Harding, S., Pettigrew, G. W., and Moura, I. (2003) Ca<sup>2+</sup> and the bacterial peroxidases: The cytochrome *c* peroxidase from *Pseudomonas stutzeri*. *JBIC, J. Biol. Inorg. Chem.* 8, 29–37.
- (9) Hoffmann, M., Seidel, J., and Einsle, O. (2009) CcpA from *Geobacter sulfurreducens* is a basic di-heme cytochrome *c* peroxidase. *J. Mol. Biol.* 393, 951–965.
- (10) Seidel, J., Hoffmann, M., Ellis, K. E., Seidel, A., Elliott, S. J., and Einsle, O. (2012) MacA is a Second Cytochrome *c* Peroxidase of *Geobacter sulfurreducens*. *Biochemistry* 51, 2747–2756.
- (11) Schutz, B., Seidel, J., Sturm, G., Einsle, O., and Gescher, J. (2011) Investigation of the electron transport chain to and the catalytic activity of the di-heme cytochrome *c* peroxidase CcpA of *Shewanella oneidensis*. *Appl. Environ. Microbiol.* 77, 6172–6180.
- (12) Shimizu, H., Schuller, D. J., Lanzilotta, W. N., Sundaramoorthy, M., Arciero, D. M., Hooper, A. B., and Poulos, T. L. (2001) Crystal structure of *Nitrosomonas europaea* cytochrome *c* peroxidase and the structural basis for ligand switching in bacterial di-heme peroxidases. *Biochemistry* 40, 13483–13490.
- (13) Pauleta, S. R., Cooper, A., Nutley, M., Errington, N., Harding, S., Guerlesquin, F., Goodhew, C. F., Moura, I., Moura, J. J., and Pettigrew, G. W. (2004) A copper protein and a cytochrome bind at the same site on bacterial cytochrome *c* peroxidase. *Biochemistry* 43, 14566–14576.
- (14) Pettigrew, G. W., Goodhew, C. F., Cooper, A., Nutley, M., Jumel, K., and Harding, S. E. (2003) The electron transfer complexes of cytochrome *c* peroxidase from *Paracoccus denitrificans*. *Biochemistry* 42, 2046–2055.
- (15) Zahn, J. A., Arciero, D. M., Hooper, A. B., Coats, J. R., and DiSpirito, A. A. (1997) Cytochrome *c* peroxidase from *Methylococcus capsulatus* Bath. *Arch. Microbiol.* 168, 362–372.
- (16) Echalié, A., Brittain, T., Wright, J., Boycheva, S., Mortuza, G. B., Fulop, V., and Watmough, N. J. (2008) Redox-linked structural changes associated with the formation of a catalytically competent form of the di-heme cytochrome *c* peroxidase from *Pseudomonas aeruginosa*. *Biochemistry* 47, 1947–1956.
- (17) De Smet, L., Pettigrew, G. W., and Van Beeumen, J. J. (2001) Cloning, overproduction and characterization of cytochrome *c* peroxidase from the purple phototrophic bacterium *Rhodobacter capsulatus*. *Eur. J. Biochem.* 268, 6559–6568.
- (18) Pulcu, G. S., Frato, K. E., Gupta, R., Hsu, H. R., Levine, G. A., Hendrich, M. P., and Elliott, S. J. (2012) The Diheme Cytochrome *c* Peroxidase from *Shewanella oneidensis* Requires Reductive Activation. *Biochemistry* 51, 974–985.
- (19) Ellfolk, N., Ronnberg, M., Aasa, R., Andreasson, L. E., and Vanngard, T. (1983) Properties and function of the two hemes in *Pseudomonas* cytochrome *c* peroxidase. *Biochim. Biophys. Acta* 743, 23–30.
- (20) Pettigrew, G. W., Prazeres, S., Costa, C., Palma, N., Krippahl, L., Moura, I., and Moura, J. J. (1999) The structure of an electron transfer complex containing a cytochrome *c* and a peroxidase. *J. Biol. Chem.* 274, 11383–11389.
- (21) Pettigrew, G. W., Pauleta, S. R., Goodhew, C. F., Cooper, A., Nutley, M., Jumel, K., Harding, S. E., Costa, C., Krippahl, L., Moura, I., and Moura, J. (2003) Electron transfer complexes of cytochrome *c* peroxidase from *Paracoccus denitrificans* containing more than one cytochrome. *Biochemistry* 42, 11968–11981.
- (22) Arciero, D. M., and Hooper, A. B. (1994) A di-heme cytochrome *c* peroxidase from *Nitrosomonas europaea* catalytically active in both the oxidized and half-reduced states. *J. Biol. Chem.* 269, 11878–11886.
- (23) Krissinel, E., and Henrick, K. (2007) Inference of macromolecular assemblies from crystalline state. *J. Mol. Microbiol.* 372, 774–797.
- (24) Schutz, B., Seidel, J., Sturm, G., Einsle, O., and Gescher, J. (2011) Investigation of the electron transport chain to and the catalytic activity of the di-heme cytochrome *c* peroxidase CcpA of *Shewanella oneidensis*. *Appl. Environ. Microbiol.* 77, 6172–6180.



- (25) Philo, J. S. (2000) A method for directly fitting the time derivative of sedimentation velocity data and an alternative algorithm for calculating sedimentation coefficient distribution functions. *Anal. Biochem.* 279, 151–163.
- (26) Rai, N., Nollmann, M., Spotorno, B., Tassara, G., Byron, O., and Rocco, M. (2005) SOMO (SOLution MOdeler) differences between X-ray- and NMR-derived bead models suggest a role for side chain flexibility in protein hydrodynamics. *Structure* 13, 723–734.
- (27) Schuetz, B., Schicklberger, M., Kuermann, J., Spormann, A. M., and Gescher, J. (2009) Periplasmic electron transfer via the c-type cytochromes MtrA and FccA of *Shewanella oneidensis* MR-1. *Appl. Environ. Microbiol.* 75, 7789–7796.
- (28) Moore, G. R., and Pettigrew, G. W. (1990) *Cytochromes c: Evolutionary, structural, and physicochemical aspects*, Springer-Verlag, Berlin.
- (29) Gilmour, R., Goodhew, C. F., Pettigrew, G. W., Prazeres, S., Moura, I., and Moura, J. J. (1993) Spectroscopic characterization of cytochrome c peroxidase from *Paracoccus denitrificans*. *Biochem. J.* 294, 745–752.
- (30) Foote, N., Peterson, J., Gadsby, P. M., Greenwood, C., and Thomson, A. J. (1985) Redox-linked spin-state changes in the di-haem cytochrome c-551 peroxidase from *Pseudomonas aeruginosa*. *Biochem. J.* 230, 227–237.
- (31) Foote, N., Peterson, J., Gadsby, P. M., Greenwood, C., and Thomson, A. J. (1984) A study of the oxidized form of *Pseudomonas aeruginosa* cytochrome c-551 peroxidase with the use of magnetic circular dichroism. *Biochem. J.* 223, 369–378.
- (32) Dias, J. M., Alves, T., Bonifacio, C., Pereira, A. S., Trincão, J., Bourgeois, D., Moura, I., and Romão, M. J. (2004) Structural basis for the mechanism of Ca<sup>2+</sup> activation of the di-heme cytochrome c peroxidase from *Pseudomonas nautica* 617. *Structure* 12, 961–973.
- (33) Fulop, V., Ridout, C. J., Greenwood, C., and Hajdu, J. (1995) Crystal structure of the di-haem cytochrome c peroxidase from *Pseudomonas aeruginosa*. *Structure* 3, 1225–1233.
- (34) Jaffe, E. K. (2005) Morpheins: A new structural paradigm for allosteric regulation. *Trends Biochem. Sci.* 30, 490–497.
- (35) Balch, W. E., Morimoto, R. I., Dillin, A., and Kelly, J. W. (2008) Adapting proteostasis for disease intervention. *Science* 319, 916–919.
- (36) Selwood, T., and Jaffe, E. K. (2012) Dynamic dissociating homo-oligomers and the control of protein function. *Arch. Biochem. Biophys.* 519, 131–143.
- (37) He, M. M., Smith, A. S., Oslob, J. D., Flanagan, W. M., Braisted, A. C., Whitty, A., Cancilla, M. T., Wang, J., Lugovskoy, A. A., Yoburn, J. C., Fung, A. D., Farrington, G., Eldredge, J. K., Day, E. S., Cruz, L. A., Cachero, T. G., Miller, S. K., Friedman, J. E., Choong, I. C., and Cunningham, B. C. (2005) Small-molecule inhibition of TNF- $\alpha$ . *Science* 310, 1022–1025.
- (38) Hayouka, Z., Rosenbluh, J., Levin, A., Loya, S., Lebendiker, M., Veprintsev, D., Kotler, M., Hizi, A., Loyter, A., and Friedler, A. (2007) Inhibiting HIV-1 integrase by shifting its oligomerization equilibrium. *Proc. Natl. Acad. Sci. U.S.A.* 104, 8316–8321.
- (39) Sirover, M. A. (1999) New insights into an old protein: The functional diversity of mammalian glyceraldehyde-3-phosphate dehydrogenase. *Biochim. Biophys. Acta* 1432, 159–184.
- (40) Jeffery, C. J. (2009) Moonlighting proteins: An update. *Mol. Biosyst.* 5, 345–350.